

**Single-Atom Implanted Two-dimensional MOFs as Efficient  
Electrocatalysts for Oxygen Evolution Reaction**

Journal:	<i>Inorganic Chemistry Frontiers</i>
Manuscript ID	QI-CMT-07-2020-000812.R1
Article Type:	Research Article
Date Submitted by the Author:	17-Sep-2020
Complete List of Authors:	Peng, Rui-li; Huazhong UniVersity of Science and Technology Li, Jialuo; Texas A&M University, Chemistry Wang, Xiao-Ning; Luoyang Normal University, Zhao, Yu-Meng; Huazhong Univ Sci Li, Bao; Huazhong Univ Sci , ; huazhong university of science and technology Xia, Bao Yu; Huazhong University of Science and Technology, School of Chemistry and Chemical Engineering Zhou, Hong-Cai; Texas A&M University, Chemistry



Journal Name

ARTICLE

## Single-Atom Implanted Two-dimensional MOFs as Efficient Electrocatalysts for Oxygen Evolution Reaction

Rui-Li Peng<sup>a</sup>, Jia-Luo Li<sup>b</sup>, Xiao-Ning Wang<sup>a</sup>, Yu-Meng Zhao<sup>a</sup>, Bao Li<sup>a,\*</sup>, Bao Yu Xia<sup>a,\*</sup> and Hong-Cai Zhou<sup>b,c,\*</sup>

Received 00th January 20xx,  
Accepted 00th January 20xx

DOI: 10.1039/x0xx00000x

[www.rsc.org/](http://www.rsc.org/)

**Abstract:** The exploration of novel electrochemical energy conversion and storage devices has been extensively studied in recent decades for their specific advantages. Therefore, the design of highly efficient, stable, and noble-metal-free electrocatalysts for oxygen-related reactions (OER) is critical but challenging, which is still worth improving. Herein, a facile and controllable synthesis strategy for bimetallic electrocatalysts for OER from a two-dimensional iron-based Metal-Organic Framework (HUST-8, HUST = Huazhong University of Science and Technology) precursor had been reported. The unoccupied porphyrin center had been disposed into the layer structure of HUST-8, which is very facile for the introduction of second types of metal center via post-modified treatment. Guided by the synthesis strategy, Fe/Ni, Fe/Co, Fe/Zn, Fe/Mn and Fe/Fe species had been fabricated, and their electrocatalytic performance for OER had been further characterized, in which Fe/Ni type exhibits the best efficiency and conversion. For Fe/Ni species of HUST-8 (labeled as Ni@HUST-8), in 1M KOH, the initial potential for OER activity performance is 170mV (vs RHE). At 10 mA cm<sup>-2</sup>, the corresponding overpotential is 240mV and the slope of Tafel is simulated as 60.8 mv dec<sup>-1</sup>. All of these experimental results of Ni@HUST-8 illustrate the better performance than commercial IrO<sub>2</sub>. Compared to the MOF parent and other bimetallic species, the higher electrocatalytic performance of Ni@HUST-8 should be ascribed to the special synergistic effect of Fe and Ni centers, which tends to greatly improve reaction kinetics and charge transfer efficiency, while increase the activity of OER and achieve the best catalytic performances. The systematical investigation clearly manifest the important role of synergistic effect of bimetallic centers towards OER, and explore the other insight into fabricating the tailored electrocatalysts derived from MOF-based templates.

### Introduction

Nowadays, the severe challenge of energy and environmental crisis has evoked the urgent requirements for the environmental-friendly and sustainable energy and the related conversion devices.<sup>1,2</sup> Electrochemical decomposition of water has been well recognized as an effective way to generate clean and renewable energy in acidic, neutral and alkaline media.<sup>3</sup> Compared to the reactions occurred in alkaline electrolyzers, the process in the acidic proton exchange membrane electrolyzer has shown the special advantages of low resistance and high efficiency. Additionally, its corresponding anodic oxygen evolution reaction (OER) should be of the limiting factor for achieving the highly efficient performances. OER is sluggish half reaction that undergoes not only a four-electron transfer process, but also the adsorption and desorption of a variety of intermediates, and finally decompose water molecules into oxygen.<sup>4,5</sup> Utilization of proper electrocatalysts and deeper exploration of structural-activity relationship of OER would be very facile to prompt the progress of hydrogen generation technology.<sup>6-9</sup> RuO<sub>2</sub> and IrO<sub>2</sub> acted as the electrocatalysts for OER with high catalytic activity had been explored. However, there are several severe drawbacks which inevitably limit their wide applications in industry: the precious metal resources are scarce and

<sup>a</sup> Key Laboratory of Material Chemistry for Energy Conversion and Storage, School of Chemistry and Chemical Engineering, Huazhong University of Science and Technology, Wuhan, Hubei, 430074, PR China. E-mail: libao@hust.edu.cn.

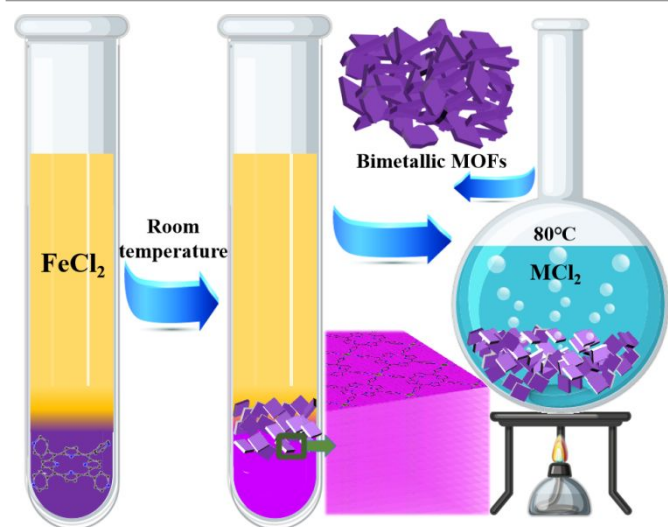
<sup>b</sup> Department of Chemistry, Texas A&M University, College Station, Texas 77843-3255, United States.

<sup>c</sup> Department of Materials Science and Engineering, Texas A&M University, College Station, Texas 77842, United States.

† Electronic Supplementary Information (ESI) available. CCDC 2011238. For ESI and crystallographic data in CIF or other electronic format see DOI: 10.1039/x0xx00000x

expensive, are facile to be poisoned caused by the fuel crossover effect, and may suffer from agglomeration and leaching after long-term usage.<sup>10, 11</sup> Therefore, it is necessary to prepare alternative electrode materials with high stability and activity that consisted of inexpensive metallic components.<sup>12-16</sup>

To date, several types of alternative active materials such as metal oxides, hydroxides or their related composites had been explored, while their corresponding electrocatalytic performances had manifested the great the feasibility as OER electrocatalysts.<sup>17, 18 19-22</sup> One of the major challenges of these current systems includes the effective preparation of single atom implanted electrocatalysts with high efficiency and conversion.<sup>23-25</sup> Additionally, iron-based electrocatalysts have also attracted much attention due to their activity and rich resources, but the materials with single iron states usually present poor performance due to their inactivation and unsatisfactory structure.<sup>26-29</sup> Utilization of Metal-Organic Frameworks (MOFs), the observed shortcomings could be surmounted since the structural advantages of MOFs as variable components and tunability. Through various treatments, MOFs-based electrocatalysts have been extensively developed, and relevant progress has been achieved.<sup>30-34</sup> Recently, two-dimensional (2D) MOFs have been considered to be of the model electrocatalysts because of their porous structure, fast transfer velocities of ions through the thickness, and large ratio of exposed active sites.<sup>35-37</sup>



**Scheme 1.** the gentle synthesis route of bimetallic MOFs via two moderate step, in which M stands for Mn, Fe, Co, Ni or Zn ion.

On the other hand, it had been validated that the introduction of bimetallic centers is very beneficial to improve the related electrocatalytic performance, even with trimetallic species.<sup>38, 39</sup> The hybridization of different metallic centers could provide an synergistic effect to improve the related electrocatalytic performances. But most of the bimetallic catalysts are prepared under high temperature or extreme treatment, the energy efficient and environmentally friendly systems are rarely developed. With the above considerations in mind, how to effectively prepare 2D MOFs containing

composite metal centers as electrocatalysts for OER and explore their catalytic mechanisms and structure-activity relationship in detail, which has become the key to solving the development problems in the current field.<sup>40, 41</sup> Herein, a new 2D MOF, [FeCl<sub>2</sub>(L)] (HUST-8, L = 5,10,15,20-Tetrakis(4-pyridyl)porphyrin, HUST = Huazhong University of Science and Technology), had been fabricated under room temperature, which consists of unoccupied porphyrin centers. The different types of second metal ions could be implanted moderately into 2D parents (shown in Scheme 1). After the characteristics of electrocatalytic performances of catalysts post-modified with different metal centers, Ni@HUST-8 exhibits the best results. The synthesis, crystal structure, electrocatalytic results and theoretical calculations of mechanism had been detailed.

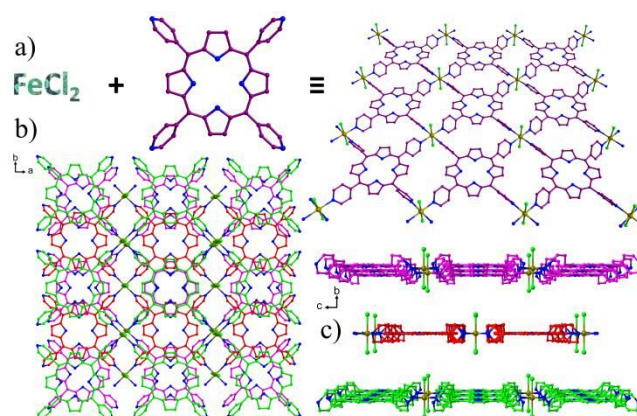


**Figure 1.** (a) The components of HUST-8, showing 2D layer structure with empty sites; (b) 3D packing mode showing ABA mode; (c) The distance of the adjacent layers.

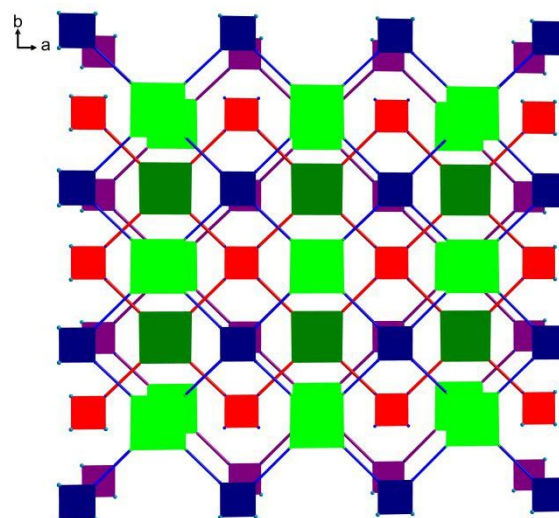


**Figure 2.** Topological structure of HUST-8.

## Results and discussion

### Crystal Structure of HUST-8

The parent 2D Fe-MOF had been synthesized via diffusion method by FeCl<sub>2</sub> salt and tetrapyrinate ligand L. The square crystal samples had been obtained after two weeks. Due to the layer structure of crystal samples, high crystalline quality of

crystal samples is difficult to obtain. After several attempts, the satisfied crystal data of final samples had been achieved at low temperature. Single crystal X-ray diffraction data had been gathered in Table S1-S2. HUST-8 crystallizes in monoclinic space group  $P2_1/c$ , whose asymmetric unit contains one iron center, one chloride and one half ligand. Each iron center adapts the octahedral configuration which is surrounded by two chlorides and four pyridyl rings of different ligands. The bond lengths of Fe-N and Fe-Cl bonds fall in the ranges of 2.229(1) to 2.439(2) Å, in consistent with the typical values of Fe (II) states. Furthermore, each tetrapyrridyl ligand connects four iron centers in one plane to fabricate 2D framework in the  $ab$  plane (Figure 1). The center of porphyrin center had been preserved into the layer framework due to the adaption of room temperature reaction conditions, which is very facile for the introduction of different metal centers via post-modified routine. The adjacent layers stack with each other in "ABA" mode (Figure 1) to facilitate the final 3D packing structures, which leaves large channels between the adjacent layers (Figure S1). Within a sheet, the shortest Fe...Fe distance is about 13.959(2) Å. Additionally, the distance between adjacent layers is measured as 8.472(3) Å, while the distance between interval layers is 16.788(2) Å. Calculated by *PLATON* program, the solvent accessible volume in HUST-8 has been evaluated as 54.8%. Considering the central iron centers and tetrapyrridyl ligands as four-connecting nodes, the layer framework of HUST-8 topologically exhibits a 4-connected uninodal *sql/Shubnikov* network with the point (Schläfli) symbol  $\{4^4 \cdot 6^2\}$  calculated with *TOPOS* software (Figure 2). Thus interleaved *sql/Shubnikov* tetragonal plane net stack over each other to form a [4] tiling structure with plane net signature of  $[122]_4[4 \cdot 4 \cdot 4 \cdot 4]$ .

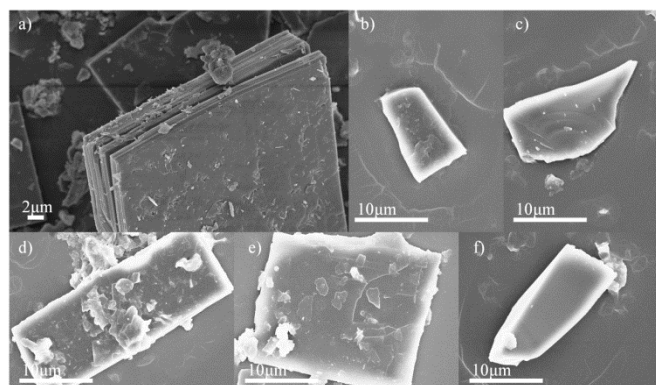


**Figure 3.** SEM images for (a) HUST-8; (b) Fe@HUST-8; (c) Co@HUST-8; (d) Ni@HUST-8; (e) Mn@HUST-8; and (f) Zn@HUST-8.

### Synthesis of the bimetallic systems

The characteristics of 2D layered structure of HUST-8 determine that the crystal samples should exhibit flake stacking traits, which could be confirmed by scanning electron microscope (SEM) photo. As shown in Figure 3a, the morphology of square sheet had been observed, while the thickness of the sheet is about 100 nm, corresponding to the accumulation of 2D frameworks.

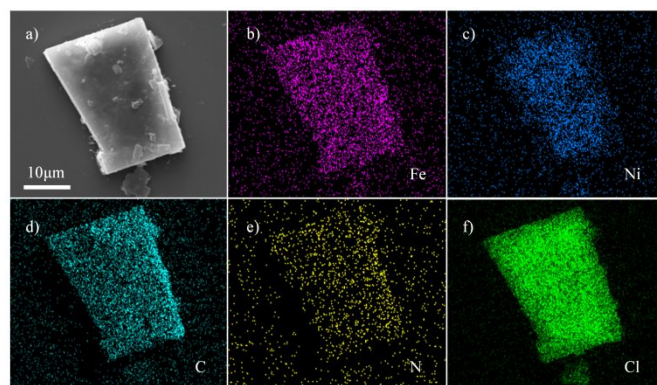


**Figure 4.** The morphology and element analysis of Ni@HUST-8: (a) SEM image; and (b-f) STEM-EDS mapping images.

Moreover, one sheet obviously consists of several flake pieces, which might be responsible for the low quality of crystal data. In addition, the existence of unoccupied porphyrin centers could be disposed with different metal ions via moderate treatments. Crystal samples of HUST-8 and different metal chlorides had been immersed and refluxed in chloroform overnight, and the resulted samples had been filtered and dried to obtain the hierarchical samples as Ni@HUST-8, Co@HUST-8, Zn@HUST-8, Mn@HUST-8 and Fe@HUST-8, which were directly utilized for structural and electrocatalytic characterizations.

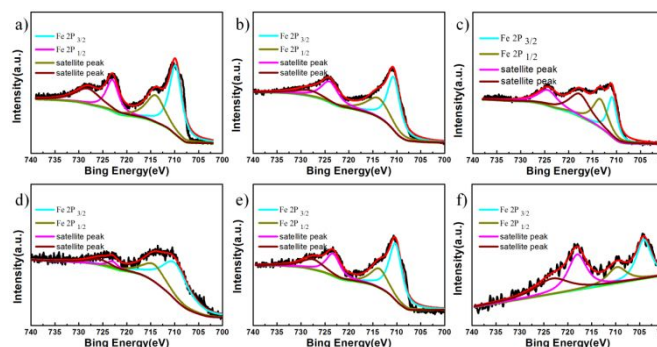


**Figure 5.** The XPS spectra of Fe 2p in different samples: (a) HUST-8; (b) Fe@HUST-8; (c) Co@HUST-8; (d) Ni@HUST-8; (e) Mn@HUST-8; and (f) Zn@HUST-8.

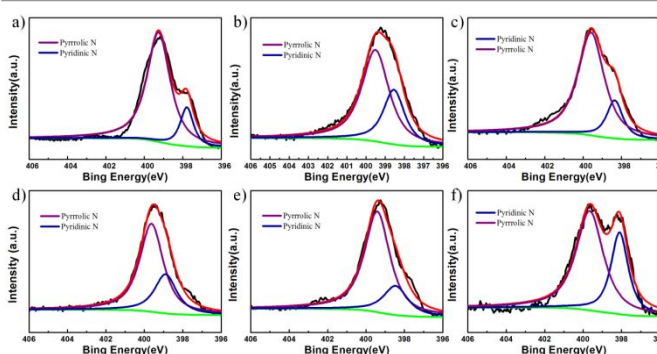


**Figure 6.** The XPS spectra of N in different samples: (a) HUST-8; (b) Fe@HUST-8; (c) Co@HUST-8; (d) Ni@HUST-8; (e) Mn@HUST-8; and (f) Zn@HUST-8.

After the programmable treatment, the hierarchical bimetallic products not only preserve the integrity of the

original framework, but also maintain the square morphology, which could be visualized via the observation of SEM (Figure 3) and power XRD patterns (Figure S3). The morphologies of some square samples had been broken due to the post-modified treatment, and the layered frameworks had been exploited and broken. More importantly, the different anticipated metal elements had been introduced and uniformly distributed in the fabricated hybrid materials with the controllable ratio, which had been validated via element energy dispersive spectrometer (EDS) mapping. For example, in Ni@HUST-8, the elements of Fe/Ni/C/N/Cl distribute evenly in the whole sample (Figure 4). No concentration area of single element could be detected, illustrating no metal oxide or aggregated metal state resided in Ni@HUST-8. In addition, the ratio of Ni and Fe elements was simulated as 1.2:1 via the semi-quantitative analysis of EDS, which was close to the theoretical values. The similar distribution of versatile elements could be also observed in other bimetallic samples, which had been listed in Figure S4 and Table S3. Via XRD patterns, the basic framework could be still preserved. The deviations between the original framework and hierarchical bimetallic samples might be caused by the introduction of secondary metal centers or the exploitation of layer frameworks. The broken of the original 2D framework might cause the change of the diffraction peaks and positions, and result in the described XRD patterns.

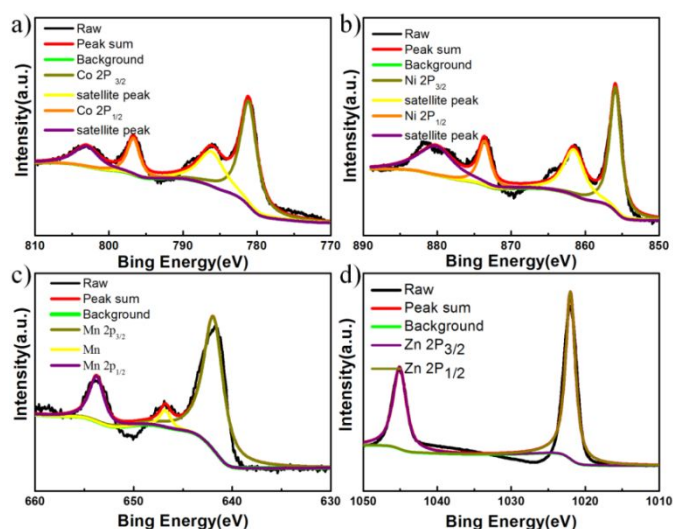


**Figure 7.** The XPS spectra of the second metal in different samples: (a) Co@HUST-8; (b) Ni@HUST-8; (c) Mn@HUST-8; and (d) Zn@HUST-8.

In order to further characterize the state of compositions, X-ray photoelectron spectroscopy (XPS) measurements were performed for hierarchical bimetallic materials (Figure 5-7). For each system, the positions of iron, chlorine and pyridyl-nitrogen peaks changed slightly compared to the template one. The extraneous existences of the secondary metal centers fully illustrate the successful introduction of the secondary metallic centers into the original iron scaffold. Additionally, the corresponding configurations of secondary metal peaks in XPS patterns manifest the divalent metal state. Comparably, the

apparent changes of electron binding energies could be presented for porphyrin nitrogen. The different binding interactions caused by the disposed secondary metal centers must be responsible for the deviations compared to the unoccupied template, which also illustrates the successful introduction of bimetallic centers into the original iron template.

#### Electrocatalytic performances of different samples

The structural characteristics of these hierarchical materials as 2D sheet, porous frameworks and bimetallic centers provide the great possibilities as electrocatalysts in OER reactions. Therefore, the systematic OER activities had been carried out to explore the potential possibilities. The corresponding OER experiments had been measured in 1M KOH electrolyte and three-electrode system. Linear-sweep-voltammetry (LSV) had been listed in Figure 8a. The inclusion of the secondary metallic centers would enhance the related OER activities compared to the tiny efficient of the original iron MOF. Co@HUST-8 and Ni@HUST-8 exhibit the better performances than the standard IrO<sub>2</sub> material, while Ni@HUST-8 behaves the best OER activity. For Ni@HUST-8, the overpotential is measured as 240mV to reach the current density of 10 mA cm<sup>-2</sup> that is the standard for evaluating the performance of OER activities, which is better than Co@HUST-8 (270mV), IrO<sub>2</sub> (310mV), Zn@HUST-8 (309mV), Fe@HUST-8 (340mV), Mn@HUST-8 (485mV) and HUST-8 (581mV). Additionally, the simulated Tafel curves from LSV curves illustrate the similar electrocatalytic OER dynamics (Figure 8b). For Ni@HUST-8, the Tafel slope is calculated as 60.8 mV/dec, better than Co@HUST-8 (62.5mV/dec), IrO<sub>2</sub> (83.1mV/dec), Zn@HUST-8 (84.5mV/dec), Fe@HUST-8 (66.5mV/dec), Mn@HUST-8 (240.8mV/dec) and HUST-8 (263.3mV/dec). Furthermore, the turnover frequency (TOF) value of Ni@HUST-8 also demonstrates the excellent performance compared to other ones (Table S8).

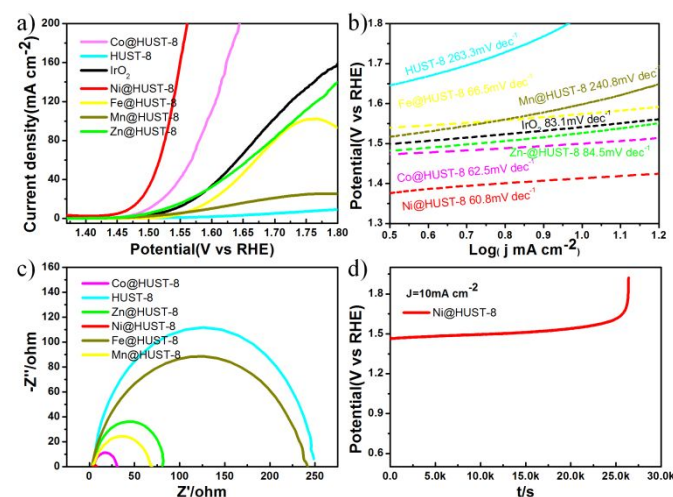


**Figure 8.** The electrochemical test results of various samples toward OER: (a) LSV plots; (b) Tafel slopes; (c) EIS spectra; and (d) Chronopotentiometry tests for Ni@HUST-8

The similar tendency of electrocatalytic performance in these hierarchical materials could be also validated via

electrochemical impedance spectroscopy (EIS). After the introduction of the different metal centers into iron scaffold, the related resistance had been significantly lowered, and Ni@HUST-8 exhibits the lowest values, which is very beneficial for charge transfer and speeding up the reaction kinetics. Viewed from the structural characteristics, the lower EIS parameters should be ascribed to the following reasons: the post-introduced metal ions have occupied the empty porphyrin centers located on the surface of layered framework, which could originate the different synergistic effect and improve the transfer environment of ions; the nitrogen-rich surface of the hybrid materials is also very conducive to the electron transfer of the catalyst and thereby accelerates the rate of electrocatalytic reaction rate. In addition, the stability test of Ni@HUST-8 was carried out by chronopotentiometry at constant current density of  $10 \text{ mA cm}^{-2}$ . As shown in Figure 8d, the potential of Ni@HUST-8 could maintain up to 25000 s and then increased rapidly, indicating the good stability of Ni@HUST-8 under the above test conditions. All in all, concluded from these electrocatalytic results, Ni@HUST-8 is validated as one promising alternative material for OER applications.

The detailed state of Ni@HUST-8 after electrocatalysis had been further investigated in order to explore the possible mechanism of pristine MOFs. PXRD spectra reveal the crystalline state had been destroyed, and only the peak position of C substance had been observed (wide peak of  $20\text{-}30^\circ$ , Figure S5). Via SEM characterizations, the layer structure of post-modified substances had been destroyed (Figure 9a), which might be caused by the ultrasound treatment or the escape of oxygen bubbles generated during catalytic process. To some extent, the aggregation of Ni and Fe elements had been presented in some area after catalysis, but most of metal elements still locate uniformly due to the restraints of framework (Figure 9). The partial aggregation of metal elements could be also observed in TEM. Furthermore, valence state of Ni (II) and Fe (II) could be validated by XPS characterization (Figure S6). Two types of N elements are still located in the substances after catalysis. Observed from all the elements distributions in the substances after catalysis, the uniform configuration might be the main responsible for the excellent catalytic properties for Ni@HUST-8.

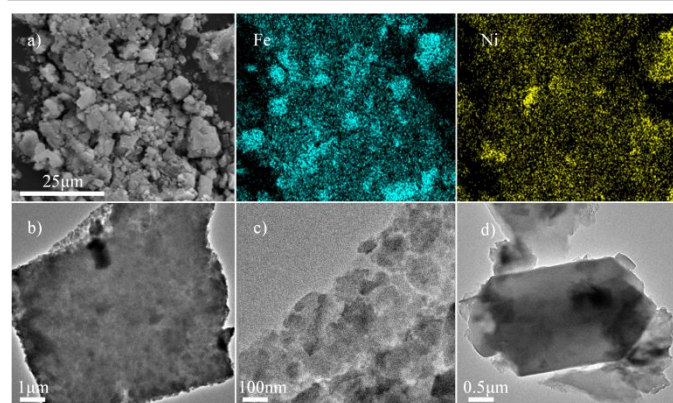


Figure 9. SEM(a) and TEM(b), (c) of Ni@HUST-8 after catalysis; TEM(d) of Ni@HUST-8.

### Theoretical Calculation of Electrocatalytic Process

In order to identify the electrocatalytic mechanism, density functional theory calculations were performed by using VASP program<sup>42</sup>. The 2D MOF had been simplified as one nickel center capped in porphyrin center and one iron center surrounded by four pyridyl rings and two chloride ions. The different active materials,  $\text{H}_2\text{O}$ ,  $\text{OH}$ ,  $\text{O}$  and  $\text{HOO}$ , are inferred as the intermediate states during the electrocatalytic process, which could be adsorbed onto the nickel ions via open metal sites. The related adsorption configurations had been setup, while the stable ones had been listed in Figure 10. With the careful considerations, the weak adsorption between  $\text{H}_2\text{O}$  and Ni ion ( $2.415 \text{ \AA}$ ,  $E_{\text{ads}} = -0.419 \text{ eV}$ ) had been presented compared to other stronger interactions ( $E_{\text{ads}} = -2.205 \text{ eV}$  for  $\text{O}$ ,  $-1.484 \text{ eV}$  for  $\text{OH}$ ,  $-1.033 \text{ eV}$  for  $\text{HOO}$ ). Bader charge analysis results reveal that electron-transferring value of Ni are  $0.89e$  for  $\text{H}_2\text{O}$ ,  $1.20e$  for  $\text{O}$  and  $1.07e$  for  $\text{OH}$  and  $\text{HOO}$  (Figure S9), in consistent with the results of adsorption energy. Charge density difference of adsorption configuration (Figure S10) had been also calculated to confirm charge transfer occurring between adsorption species and Ni atom, Cl atom and Fe atom. For the adsorption of single  $\text{O}$  atom, the highest electron transfer density between  $\text{O}$  and Ni had been observed, leading to the shortest O-Ni bond length and largest energy of the O-Ni bond. The similar electron transfer density between Cl and Fe had been also observed.

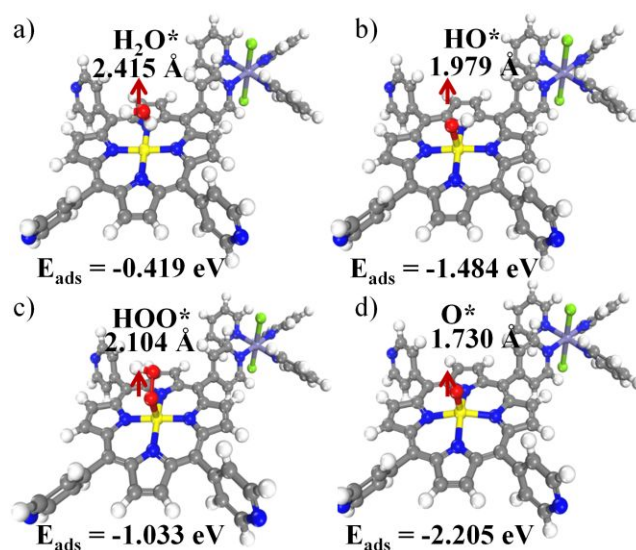


Figure 10. Optimized structure and adsorption energy of  $\text{H}_2\text{O}$  (a),  $\text{OH}$  (b),  $\text{HOO}$  (c),  $\text{O}$  (d) on Ni@HUST-8. (The color codes: H white; C brown; N blue; O red; Cl green; Ni yellow; Fe Light stone grey)

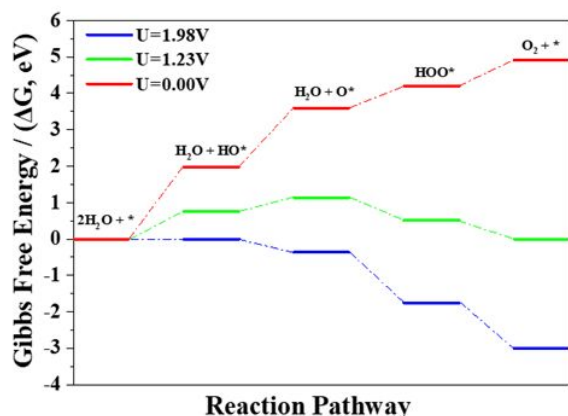


Figure 11. The calculated free energy of the Ni@HUST-8 for 4e<sup>-</sup> OER reaction.

Additionally, the free energy for 4e<sup>-</sup> OER process had further calculated with the participation of Ni@HUST-8 as the catalyst, which is listed in Figure 11. For O<sub>2</sub> formation, the change of Gibbs free energy was computed at zero potential with the red curve ( $\Delta G_1 = 1.98$  eV,  $\Delta G_2 = 1.62$  eV,  $\Delta G_3 = 0.60$  eV,  $\Delta G_4 = 0.72$  eV for the formation of HO\*, O\*, HOO\* and O<sub>2</sub>, respectively). Therefore, the rate-determined step is the formation of HO\* with  $\Delta G_{\max} = 1.98$  eV. For the ideal catalyst, the equilibrium potential of the 4e<sup>-</sup> mechanism reaction is 1.23 V in acid solution. Therefore, at the U = 1.23 V, the first step is uphill ( $\Delta G = 0.75$  V) is realized, indicating the overpotential of 0.75 V for 4e<sup>-</sup> OER reaction (green curve). Through the theoretical calculation, the feasibility of materials as electrocatalyst has been verified, and the possible electrocatalysis mechanism has been also described.

## Conclusions

In summary, a 2D MOF-based scaffold had been carefully constructed, which possess the unoccupied porphyrin centers. While the fabricated scaffold could be post-modified by different metal ions under mild conditions. The structural characteristics of 2D MOFs endow the possibility of electrocatalyst in OER, but the low OER activity had been exhibited due to the low electronic conductivity. After the post-introduction of different metal ions disposed in the empty porphyrin center, the conductivity of hybrid materials had been improved, while the electrocatalytic performance in OER had been also enhanced. Especially for Ni-containing sample, the best OER activity had been exhibited, along with an overpotential of 0.24 V, Tafel slope of 60.8 mV/dec, and the proper stability similar to IrO<sub>2</sub>. The post-modified MOF would significantly increase the exposing active sites, improve reaction kinetics and charge transfer efficiency, which are beneficial for enhancing the corresponding OER performances. All of these research results imply the great potential of the related hybrid results in metal-air cells and water separation devices, and provide further reference for the application of electrochemical energy science.

## Conflicts of interest

There are no conflicts to declare.

## Acknowledgements

We must thank Dr. Gui-Lin Zhuang for theoretical calculation. This work was supported by the financial supports of National Science Foundation of China ( 21971078, 21471062 ), the Center for Gas Separations Relevant to Clean Energy Technologies, an Energy Frontier Research Center (EFRC) funded by the U.S. Department of Energy (DOE), Office of Science, and Office of Basic Energy Sciences (DESC0001015), Office of Fossil Energy, the National Energy Technology Laboratory (DE-FE0026472), the Robert A. Welch Foundation through a Welch Endowed Chair to HJZ (A-0030), the Fundamental Research Funds for the Central Universities (2019kfyRCPY071, 2019kfyXKJC009), and the Frontier Project of Application Foundation of Wuhan Science and Technology Bureau of China (Grant No. 2020010601012201). We gratefully acknowledge the Analytical and Testing Center, Huazhong University of Science and Technology, for analysis and spectral measurements. We also thank the staffs from BL17B beamline of the National Center for Protein Sciences Shanghai (NCPSS) at Shanghai Synchrotron Radiation Facility, for assistance during data collection.

## Notes and references

- Panwar, N. L.; Kaushik, S. C.; Kothari, S. Role of renewable energy sources in environmental protection: A review. *Renewable Sustainable Energy Rev.* **2011**, *15*, 1513-1524.
- Liu, S. J.; Han, S. D.; Zhao, J. P.; Xu, J.; Bu, X. H. In-situ synthesis of molecular magnetorefrigerant materials. *Coord. Chem. Rev.* **2019**, *394*, 39-52.
- Morales-Guio, C. G.; Stern, L.; Hu, X. Nanostructured hydrotreating catalysts for electrochemical hydrogen evolution. *Chem. Soc. Rev.* **2014**, *43*, 6555-6569.
- Zhu, R.; Ding, J.; Xu, Y.; Yang, J.; Xu, Q.; Pang, H.  $\pi$ -Conjugated Molecule Boosts Metal-Organic Frameworks as Efficient Oxygen Evolution Reaction Catalysts. *Small* **2018**, *14*, 1803576.
- Yuan, M.; Dipazir, S.; Wang, M.; Sun, Y.; Gao, D.; Bai, Y.; Zhang, M.; Lu, P.; He, H.; Zhu, X.; Li, S.; Liu, Z.; Luo, Z.; Zhang, G. Polyoxometalate-assisted formation of CoSe/MoSe<sub>2</sub> heterostructures with enhanced oxygen evolution activity. *J. Mater. Chem. A* **2019**, *7*, 3317-3326.
- Koper, M. T. M. Thermodynamic theory of multi-electron transfer reactions: Implications for electrocatalysis. *J. Electroanal. Chem.* **2011**, *660*, 254-260.
- Li, Z.; He, H.; Cao, H.; Sun, S.; Diao, W.; Gao, D.; Lu, P.; Zhang, S.; Guo, Z.; Li, M.; Liu, R.; Ren, D.; Liu, C.; Zhang, Y.; Yang, Z.; Jiang, J.; Zhang, G. Atomic Co/Ni dual sites and Co/Ni alloy nanoparticles in N-doped porous Janus-like carbon frameworks for bifunctional oxygen electrocatalysis. *Appl. Catal., B* **2019**, *240*, 112-121.
- Yu, X.; Feng, Y.; Guan, B.; Lou, X. W. D.; Paik, U. Carbon coated porous nickel phosphides nanoplates for highly efficient oxygen evolution reaction. *Energy Environ. Sci.* **2016**, *9*, 1246-1250.

9. He, P.; Yu, X.; Lou, X. W. D. Carbon-Incorporated Nickel-Cobalt Mixed Metal Phosphide Nanoboxes with Enhanced Electrocatalytic Activity for Oxygen Evolution. *Angew.Chem. Int.Ed.* **2017**, *56*, 3897-3900.
10. Zhang, K.; Guo, W.; Liang, Z.; Zou, R. Metal-organic framework based nanomaterials for electrocatalytic oxygen redox reaction. *Sci. China Chem.* **2019**, *62*, 417-429.
11. Jayaramulu, K.; Masa, J.; Tomanec, O.; Peeters, D.; Ranc, V.; Schneemann, A.; Zboril, R.; Schuhmann, W.; Fischer, R. A. Nanoporous Nitrogen-Doped Graphene Oxide/Nickel Sulfide Composite Sheets Derived from a Metal-Organic Framework as an Efficient Electrocatalyst for Hydrogen and Oxygen Evolution. *Adv. Funct. Mater.* **2017**, *27*, 1700451.
12. Li, F.; Wang, P.; Huang, X.; Young, D.; Wang, H.; Braunstein, P.; Lang, J. Large-Scale, Bottom-Up Synthesis of Binary Metal-Organic Framework Nanosheets for Efficient Water Oxidation. *Angew. Chem. Int. Ed.*, **2019**, *58*, 7051-7056.
13. Li, F.; Shao, Q.; Huang, X.; Lang, J. Nanoscale Trimetallic Metal-Organic Frameworks Enable Efficient Oxygen Evolution Electrocatalysis. *Angew. Chem. Int. Ed.*, **2018**, *57*, 1888-1892.
14. Xue, J.; Li, C.; Li, F.; Gu, H.; Braunstein, P.; Lang, J. Recent advances in pristine tri-metallic metal-organic frameworks toward the oxygen evolution reaction. *Nanoscale*, **2020**, *12*, 4816-4825.
15. Li, C.; Li, X.; Zhao, Z.; Li, F.; Xue, J.; Niu, Z.; Gu, H.; Braunstein, P.; Lang, J. Iron-doped NiCo-MOF hollow nanospheres for enhanced electrocatalytic oxygen evolution. *Nanoscale*, **2020**, *12*, 14004-14010.
16. Wu, T.; Pi, M.; Wang, X.; Zhang, D.; Chen, S. Three-dimensional metal-organic framework derived porous  $\text{CoP}_3$  concave polyhedrons as superior bifunctional electrocatalysts for the evolution of hydrogen and oxygen. *Phys. Chem. Chem. Phys.* **2017**, *19*, 2104-2110.
17. Cheng, F.; Shen, J.; Peng, B.; Pan, Y.; Tao, Z.; Chen, J. Rapid room-temperature synthesis of nanocrystalline spinels as oxygen reduction and evolution electrocatalysts. *Nat. Chem.* **2011**, *3*, 79-84.
18. Osgood, H.; Devaguptapu, S. V.; Xu, H.; Cho, J.; Wu, G. Transition metal (Fe, Co, Ni, and Mn) oxides for oxygen reduction and evolution bifunctional catalysts in alkaline media. *Nano Today* **2016**, *11*, 601-625.
19. Yang, J.; Zhu, G.; Liu, Y.; Xia, J.; Ji, Z.; Shen, X.; Wu, S.  $\text{Fe}_3\text{O}_4$ -Decorated  $\text{Co}_9\text{S}_8$  Nanoparticles In Situ Grown on Reduced Graphene Oxide: A New and Efficient Electrocatalyst for Oxygen Evolution Reaction. *Adv. Funct. Mater.* **2016**, *26*, 4712-4721.
20. Tang, C.; Wang, H.; Zhang, Q. Multiscale Principles To Boost Reactivity in Gas-Involving Energy Electrocatalysis. *Acc. Chem. Res.* **2018**, *51*, 881-889.
21. Kim, J. S.; Kim, B.; Kim, H.; Kang, K. Recent Progress on Multimetal Oxide Catalysts for the Oxygen Evolution Reaction. *Adv. Energy Mater.* **2018**, *8*, 1702774.
22. Han, L.; Dong, S.; Wang, E. Transition-Metal (Co, Ni, and Fe)-Based Electrocatalysts for the Water Oxidation Reaction. *Adv. Mater.* **2016**, *28*, 9266-9291.
23. Tao, L.; Lin, C.; Dou, S.; Feng, S.; Chen, D.; Liu, D.; Huo, J.; Xia, Z.; Wang, S. Creating coordinatively unsaturated metal sites in metal-organic-frameworks as efficient electrocatalysts for the oxygen evolution reaction: Insights into the active centers. *Nano energy* **2017**, *41*, 417-425.
24. Han, X.; Ling, X.; Wang, Y.; Ma, T.; Zhong, C.; Hu, W.; Deng, Y. Generation of Nanoparticle, Atomic-Cluster, and Single-Atom Cobalt Catalysts from Zeolitic Imidazole Frameworks by Spatial Isolation and Their Use in Zinc-Air Batteries. *Angew.Chem. Int.Ed.* **2019**, *58*, 5359-5364.
25. Zang, W.; Sumboja, A.; Ma, Y.; Zhang, H.; Wu, Y.; Wu, S.; Wu, H.; Liu, Z.; Guan, C.; Wang, J.; Pennycook, S. J. Single Co Atoms Anchored in Porous N-Doped Carbon for Efficient Zinc-Air Battery Cathodes. *ACS Catal.* **2018**, *8*, 8961-8969.
26. Xie, S.; Li, F.; Xu, S.; Li, J.; Zeng, W. Cobalt/iron bimetal-organic frameworks as efficient electrocatalysts for the oxygen evolution reaction. *Chin. J. Catal.* **2019**, *40*, 1205-1211.
27. Wurster, B.; Grumelli, D.; Hötger, D.; Gutzler, R.; Kern, K. Driving the Oxygen Evolution Reaction by Nonlinear Cooperativity in Bimetallic Coordination Catalysts. *J. Am. Chem. Soc.* **2016**, *138*, 3623-3626.
28. Zou, Z.; Wang, T.; Zhao, X.; Jiang, W.; Pan, H.; Gao, D.; Xu, C. Expediting in-Situ Electrochemical Activation of Two-Dimensional Metal-Organic Frameworks for Enhanced OER Intrinsic Activity by Iron Incorporation. *ACS Catal.* **2019**, *9*, 7356-7364.
29. Cao, C.; Ma, D.; Xu, Q.; Wu, X.; Zhu, Q. Semisacrificial Template Growth of Self-Supporting MOF Nanocomposite Electrode for Efficient Electrocatalytic Water Oxidation. *Adv. Funct. Mater.* **2019**, *29*, (6), 1807418.
30. Li, Z.; He, H.; Cao, H.; Sun, S.; Diao, W.; Gao, D.; Lu, P.; Zhang, S.; Guo, Z.; Li, M.; Liu, R.; Ren, D.; Liu, C.; Zhang, Y.; Yang, Z.; Jiang, J.; Zhang, G. Atomic Co/Ni dual sites and Co/Ni alloy nanoparticles in N-doped porous Janus-like carbon frameworks for bifunctional oxygen electrocatalysis. *Appl. Catal., B* **2019**, *240*, 112-121.
31. Yao, S. L.; Tian, X. M.; Li, L. Q.; Liu, S. J.; Zheng, T. F.; Chen, Y. Q.; Zhang, D. S.; Chen, J. L.; Wen, H. R.; Hu, T. L. A  $\text{Cd}^{\text{II}}$ -based metal-organic framework with *pcu* topology as turn-on fluorescent sensor for  $\text{Al}^{3+}$ . *Chem. Asian J.* **2019**, *14*, 3648-3654.
32. Yan, Y.; He, T.; Zhao, B.; Qi, K.; Liu, H.; Xia, B. Y. Metal/covalent-organic frameworks-based electrocatalysts for water splitting. *J. Mater. Chem. A* **2018**, *6*, 1595-15926.
33. Xia, Z.; Fang, J.; Zhang, X.; Fan, L.; Barlow, A. J.; Lin, T.; Wang, S.; Wallace, G. G.; Sun, G.; Wang, X. Pt nanoparticles embedded metal-organic framework nanosheets: A synergistic strategy towards bifunctional oxygen electrocatalysis. *Appl. Catal., B* **2019**, *245*, 389-398.
34. Song, W.; Teng, X.; Liu, Y.; Wang, J.; Niu, Y.; He, X.; Zhang, C.; Chen, Z. Rational construction of self-supported triangle-like MOF-derived hollow (Ni, Co) $\text{Se}_2$  arrays for electrocatalysis and supercapacitors. *Nanoscale* **2019**, *11*, 6401-6409.
35. Jia, H.; Yao, Y.; Zhao, J.; Gao, Y.; Luo, Z.; Du, P. A novel two-dimensional nickel phthalocyanine-based metal-organic framework for highly efficient water oxidation catalysis. *J. Mater. Chem. A* **2018**, *6*, 1188-1195.
36. Tian, X. M.; Yao, S. L.; Qiu, C. Q.; Zheng, T. F.; Chen, Y. Q.; Huang, H.; Chen, J. L.; Liu, S. J.; Wen, H. R. Turn-on luminescent sensor toward  $\text{Fe}^{3+}$ ,  $\text{Cr}^{3+}$  and  $\text{Al}^{3+}$  based on a Co(II) metal-organic framework with open functional sites. *Inorg. Chem.* **2020**, *59*, 2803-2810.
37. Yao, S. L.; Liu, S. J.; Tian, X. M.; Zheng, T. F.; Cao, C.; Niu, C. Y.; Chen, Y. Q.; Chen, J. L.; Huang, H.; Wen, H. R. A Zn(II)-based metal-organic framework with a rare *tcj* topology as a turn-on fluorescent sensor for acetylacetone. *Inorg. Chem.* **2019**, *58*, 3578-3581.

38. Zhang, P.; Yang, X.; Gao, W.; Hou, X.; Mi, J.; Liu, L.; Huang, J.; Dong, M.; Stampfl, C. First-principles design of bifunctional oxygen reduction and evolution catalysts through bimetallic centers in metal-organic frameworks. *Catal. Sci. Technol.* **2018**, *8*, 3666-3674.
39. Gadipelli, S.; Li, Z.; Zhao, T.; Yang, Y.; Yildirim, T.; Guo, Z. Graphitic nanostructures in a porous carbon framework significantly enhance electrocatalytic oxygen evolution. *J. Mater. Chem. A* **2017**, *5*, 24686-24694.
40. Zhang, P.; Yang, X.; Gao, W.; Hou, X.; Mi, J.; Liu, L.; Huang, J.; Dong, M.; Stampfl, C. First-principles design of bifunctional oxygen reduction and evolution catalysts through bimetallic centers in metal-organic frameworks. *Catal. Sci. Technol.* **2018**, *8*, 3666-3674.
41. Gadipelli, S.; Li, Z.; Zhao, T.; Yang, Y.; Yildirim, T.; Guo, Z. Graphitic nanostructures in a porous carbon framework significantly enhance electrocatalytic oxygen evolution. *J. Mater. Chem. A* **2017**, *5*, 24686-24694.
42. Wang, Y.; Noid, W.; Liu, P.; Voth, G. A. Effective force coarse-graining. *Phys. Chem. Chem. Phys.* **2009**, *11*, 2002-2015.